This manuscript was published as formal in:

Journal of Molecular Liquids 2018, 265, 299-306

DOI: 10.1016/j.molliq.2018.05.125

https://doi.org/10.1016/j.molliq.2018.05.125

***Title*:**

Phenothiazine based nanocrystals with enhanced solid state emission

Andrei Bejan, Luminita Marin*

"Petru Poni" Institute of Macromolecular Chemistry of Romanian Academy, Iasi, Romania

*lmarin@icmpp.ro

Abstract

The paper focuses on the preparation of phenothiazine based nanoparticles, both in liquid and solid states, by reprecipitation in water and solvent induced phase separation respectively. Polymethylmethacrylate was used as an inert matrix and polyfluorene as a luminescent matrix. The morphological features of the nanoparticles were investigated by dynamic light scattering, and SEM, AFM and POM microscopy, which revealed their supramolecular ordering as nanocrystals. Their photophysical behaviour was monitored by UV-vis and photoluminescence spectroscopy. The nanocrystals emitted green light, with higher efficiency compared to the bulk crystals, reaching an absolute quantum yield of 35 % in water, 45 % in polymethylmethacrylate, and 39 % in polyfluorene.

Keywords: phenothiazine, nanocrystals, efficient luminescence, polymethylmethacrylate, polyfluorene

Introduction

Nanoparticles are a class of nanomaterials intensely studied in the last decades due to their outstanding properties, which make them promising for optoelectronics (light emitting devices, transistors, solar cells) and bioengineering (imaging, ultrasensitive detection at molecular and cellular level, drug delivery) [1-4]. Among nanoparticles, remarkable endeavour has been directed to the development of inorganic crystals (e.g. quantum dots) and conjugated polymeric nanoparticles. On the other hand, the nanocrystals based on organic low molecular weight compounds were less studied, despite the fact that they are cheaper, biologically more compatible and environmentally safer, bringing the advantage of reversible assembling/disassembling by crystallization/dissolving processes, and thus prompting an easy recycling [5,6]. The main drawback which hampered the developing of the organic nanocrystals is the difficulty to control their morphology and to prevent their precipitation. To address both challenges, aromatic units which favour an easy crystallization should be used [5-9].

Phenothiazine is a fused heterocycle that proved an easy crystallization [10-12]. Its strong electron-donating capability made it an important building block in the chemical engineering of the highly conjugated donor-acceptor materials for optoelectronics. A literature survey reveals that the phenothiazine was extensively involved to design dyes for solar cells, while less attention was devoted to its application for organic light emitting diodes. This happens despite the fact that its butterfly geometry favours the light emission in solid state, since it prevents strong intermolecular forces, limiting by this the non-radiative decay [10-12]. The few

studies reported in literature to date, targeted mainly the obtaining of donor-acceptor polymers, with the phenothiazine units incorporated in the backbone, as an alternant moiety to an acceptor counterpart (oxadiazole, fluorene or cyano substituted aromatic rings) [13-15] or as side chains on a polyfluorene backbone [16]. Also, the phenothiazine was used as a building block for dendrimers [17] or molecules with RIR (restricted intermolecular rotation) design [18, 19]. In all cases, the quantum efficiency gave encouraging values. The most promising properties, a quantum yield of almost 60 % in thin solid films, were attained by its grafting on the polyfluorene chains *via* a flexible spacer which decoupled the donor-acceptor conjugation [16]. A critical view of these data indicates that phenothiazine is a challenging building block in designing materials for optoelectronics, which deserves further efforts for improving its performances. The progress in the optoelectronic field revealed that the quantum yield in solid state could be greatly improved by manufacturing materials as blends, nanocomposites, nanocrystals or co-crystals [2, 15, 19-23]. While extensive attention has been directed to the use of these strategies to build luminescent materials based on traditional luminophores, little interest was paid to the phenothiazine [24-27]. Considering the phenothiazine's ability to facilitate an easy crystallization when it is involved as a building block in different compounds, the obtaining of phenothiazine based nanocrystals appears as a challenge from both academic and applicative points of view.

In this contribution we report the preparation of nanocrystals based on a phenothiazine derivative bearing bromine and carbonyl units. They were obtained as water suspensions by the reprecipitation method, and as nanohybrid films by dispersing in polymethylmethacrylate and polyfluorene matrix. Their morphological features were investigated using DLS, SEM, AFM and POM technics and their photophysical behaviour was monitored by UV-vis and photoluminescence spectroscopy.

Experimental

Materials

Poly(9,9-di-n-octylfluorenyl-2,7-diyl) (99 % purity, Mn=20 000) and poly(methyl methacrylate) (99 % purity, Mn=120 000) have been purchased from Sigma-Aldrich and used as received. 7-Bromo-10-(-4-hexyloxy-phenyl)-10*H*-phenothiazine-3-carbaldehyde (**FhABr**) has been prepared in our laboratory by bromination of the corresponding formyl derivative with N-bromosuccinimide, following a published procedure [11]. The product has been obtained as yellow-greenish needle single crystals, by recrystallization from ethyl acetate.

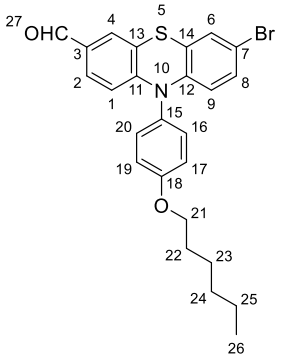

^{1}H- NMR (400.13 MHz, DMSO-d_6, ppm) δ = 9.73 (s, 1H), 7.53 (s, 1H), 7.45 (d, 1H), 7.37 (d, 2H), 7.31 (s, 1H), 7.23 (d, 2H), 7.11 (d, 1H), 6.20 (d, 1H), 6.02 (d, 1H), 4.08 (t, 2H), 1.82-1.75 (m, 2H), 1.52-1.33 (superposed bands, 6H), 0.91 (t, 3H); **^{13}C-NMR** (400.16 MHz, DMSO-d_6, ppm) δ = 190.22 (C27), 158.83 (C18), 148.21 (C11), 141.83 (C12), 131.36 (C16, C20), 131.16 (C15), 130.95 (C3), 130.02 (C4), 129.92 (C8), 128.30 (C6), 127.34 (C2), 120.58 (C14), 118.22 (C13), 117.80 (C7), 116.93 (C17, C19), 115.28 (C9), 114.89 (C1), 67.83 (C21), 30.95 (C24), 28.59 (C22), 25.17 (C23), 22.04 (C25), 13.88 (C26); **FT-IR** (KBr, cm^{-1}): 3069, 3053 ($\nu_{CHaromatic}$), 2954, 2935, 2866 (ν_{CH3}, ν_{CH2}), 1682 ($\nu_{C=O}$), 1607, 1511 ($\nu_{C=Caromatic}$), 1240 (ν_{C-O-C}), 1027 (ν_{C-Br}), 838, 803, 745 ($\delta_{CHaromatic}$); Elemental analysis calc. for $C_{25}H_{24}BrNO_2S$ (482): C 62.24, H 5.01, N 2.9, S 6.65. Found: C 62.43, H 5.21, N 3.03, S 6.71.

Nanoparticle preparation

Phenothiazine nanocrystals have been prepared by the reprecipitation method, which was chosen in order to avoid the influence of undesirable impurities, which drastically would affect their optical properties [2]. To this end, the **FhABr** solution in THF, $2x10^{-3}$ M, has been dropped into a vial containing 6 mL of water nonsolvent, under vigorous magnetic stirring, for 10 minutes. To establish the optimum concentration towards nanoparticles of best optical properties, five different volumes of **FhABr** solution were used, leading to five different systems (Table 1). The nanoparticles features were measured on fresh solutions and after one weak, in order to establish the ageing influence upon their dimensions. **FhABr** solution in THF was prepared in similar conditions and used as control sample (Table 1).

Table 1. Preparation of nanoparticles suspended in water and their codes

Code	**0**	**1**	**2**	**3**	**4**	**5**
THF solution of **FhABr** $2x10^{-3}$ M (mL)	0.05	0.01	0.02	0.03	0.04	0.05
Water (mL)	0	6	6	6	6	6
THF (mL)	6	0	0	0	0	0
Water fraction	0	99.8	99.6	99.5	99.3	99.1
FhABr in water ($x10^{-5}$ M)	-	0.33	0.66	1	1.33	1.66

Further, in order to obtain solid thin films proper for optoelectronic applications, the phenothiazine nanoparticles were dispersed into a polymeric matrix, by solution induced phase separation method [28, 29], into polymethylmethacrylate (PMMA) and polyfluorene (PF). A volume of 2 % solution of **FhABr** in toluene was slowly dropped into 6 mL of a 2 % solution of polymer in toluene under vigorous magnetic stirring (Table 2) [29]. Different volumes of **FhABr** solution (Table 2) were used, in order to reach a final concentration of the **FhABr** in polymer from 0.33 to 1.33 %, to see the influence of the concentration on the morphology and properties. The clear solutions were vigorously magnetically stirred for 10 minutes, casted onto glass lamellas, and then incubated into a closed case in order to ensure the slowly removing of the solvent in order to facilitate the **FhABr** crystallization as the polymer solution harden.

Table 2. Preparation of the polymer dispersed nanoparticles and their codes

FhABr 2 % (mL)	0	0.02	0.03	0.04	0.06	0.08	0.1
PMMA 2 % (mL)	6	6	6	6	6	6	6
Code	**PMMA**	**1a**	**2a**	**3a**	**4a**	**5a**	**6a**
PF 2% (mL)	6	6	6	6	6	6	6
Code	**PF**	**1b**	**2b**	**3b**	**4b**	**5b**	**6b**
FhABr in **PMMA/PF** (%)		0.33	0.5	0.66	1	1.33	1.66

Equipment

The size and distribution of the nanoparticles were analysed by dynamic light scattering on a Delsa Nano C, Beckman Coulter equipment, at room temperature (25 ^{o}C). The scattering light was measured at the fixed angle of 160 ^{o}C.

The phase segregation of the nanoparticles dispersed into polymeric matrix was firstly attributed with a field emission scanning electron microscope (Scanning Electron Microscope SEM EDAX – Quanta 200) at lower accelerated electron energy of 20 Kev, to avoid the sample decomposition. For a more accurate attribution of the nanoparticles dimension, atomic force microscopy images of the film samples were acquired with a Solver PRO-M, NT-MDT, Russia instrument, in semi contact mode. Nova v.1443 software was used to record and to analyse the AFM topographic and phase contrast images. To further ascribe the crystalline nature of the nanoparticles dispersed into the polymeric matrix, the samples were observed with an Olympus BH-2 polarized light microscope.

Ultraviolet–visible (UV–vis) absorption and photoluminescence (PL) spectra were recorded on a Carl Zeiss Jena SPECORD M42 spectrophotometer and Perkin Elmer LS 55 spectrophotometer, respectively, in solutions (nanoparticle suspensions) and thin films.

The fluorescence quantum yield (**QY**) and chromaticity diagrams of the nanoparticle suspensions and polymer dispersed nanoparticles were measured on a FluoroMax-4 spectrofluorometer equipped with a Quanta-phi integrating sphere accessory Horiba Jobin Yvon, by exciting at the absorption maxima, at room temperature. The slit widths and detector parameters were optimized to maximize but not saturate the excitation Rayleigh peak, in order to obtain a good optical luminescence signal-to-noise ratio.

Results and discussions

Rational design

Nanocrystals based on a phenothiazine derivative (**FhABr**) have been prepared by (i) reprecipitation in water and (ii) solvent induced phase separation methods, using as a polymer matrix polymethylmethacrylate (PMMA) and polyfluorene (PF). Three series of nanocrystals samples were obtained by varying (i) the water fraction from 99.1 up to 99.8 (coded **1-6)**, and the amount of **FhABr** from 0.33 to 1.66 % in (ii) PMMA (coded **1a-6a**) and (iii) PF (coded **1b-6b**) (Table 1, 2). Their design was thought starting from a series of premises which should allow the obtaining of multifunctional materials useful for biological and opto-electronic applications, as follows. (i) The phenothiazine has strong electron donating ability which renders it an important building block for opto-electronic materials [13-19]. (ii) Its derivatives proved a large range of biological activities and good biocompatibility, being presently studied for their antibacterial, antifungal, anticancer, antiviral, anti-inflamatory, antimalarial, anticonvulsant, analgesic, immunosuppressive, antifilarial, trypanocidal, and multidrug resistance reversal properties [30, 31]. (iii) The **FhABr** has been chosen because it emitted pure green light with a high quantum yield in solution and had the ability to easily grow as crystals from a large variety of solvents [11]. Thus, it was estimated that **FhABr** has a high potential to form nanocrystals into the water nonsolvent or into a viscous solution of polymer respectively. This should result in an increase of the surface-to-volume ratio and consequently in an improvment of the quantum yield in solid state. Moreover, combining the **FhABr** with the polyfluorene luminescent matrix, should bring the advantage of an easy manufacturing of the thin films and should raise potential synergistic effects, providing new materials with a good balance of photophysical properties. (iv) Water has been chosen as a nonsolvent because it is the friendliest biodispersant, enabling the obtaining of biocompatible materials. (v) PMMA was used as matrix for nanocrystals because it is colourless and has good insulating properties, high light transmittance, chemical resistance, low optical absorption and low cost, being an excellent inert matrix without interference from electron-transfer dynamics or emission [32]. (vi) The blue light emitting polyfluorene

has been chosen as matrix for the nanocrystals, due to its high photoluminescence in solid state which ranked it as the most prospective blue light emitting candidate for building organic light emitting diodes [33]. Previous studies reported that the combination of phenothiazine and fluorene chromophores by decoupling their conjugation led to materials with efficient luminescence in solid films [16]. Thus, by dispersing the phenothiazine chromophore into the polyfluorene matrix, materials with improved luminescence are expected to be obtained, as already demonstrated for other dyes [34]. All these premises indicated the obtaining of the phenothiazine based nanoparticles as a promising route towards bio- and opto-electronic applications.

Nanocrystals. Morphology and supramolecular arrangement

FhABr has a great potential to crystalize from a wide range of solvents due to its rigid-flexible structure which favours the segregation of phenothiazine arrays with weak π-π intermolecular distances [11] (Figure 1a). To monitor its ability of nanocrystallization by reprecipitation in water and by its dispersing into a polymeric matrix, dynamic light scattering method (DLS), scanning electron microscopy (SEM), atomic force microscopy (AFM), polarized light microscopy (POM) and fluorescence microscopy (MF) measurements were performed.

Reprecipitation of **FhABr** in water led to macroscopic clear solutions. However, DLS measurements revealed the presence of nanoparticles with mean hydrodynamic diameter from 113 to 155 nm and narrow polydispersity index from 0.09 to 0.2 (Figure 1c). The sample **3** showed the narrowest size distribution (0.098) (Table 1s), indicating the water fraction of 99.5 as being the optimum for providing homogeneous samples. By contrast, the pristine solution of **FhABr** in THF didn't reveal any nanoparticle formation. The ageing of the samples lead to an increase of the nanoparticle dimensions up to 985 nm and a polydispersity index up to 0.4 (Figure 1d, Table 1s). The samples with average amounts of **FhABr** (**2**, **3**) suffered less alteration of the dimensional parameters, suggesting once more the water fraction of 99.5 as being the best, being able to provide nanoparticles with increased stability, at least for one week.

SEM images acquired on the suspension samples casted on glass revealed a flower-like crystalline morphology of the nanoparticles highlighting their tendency of crystallization in aqueous medium (Figure 1b).

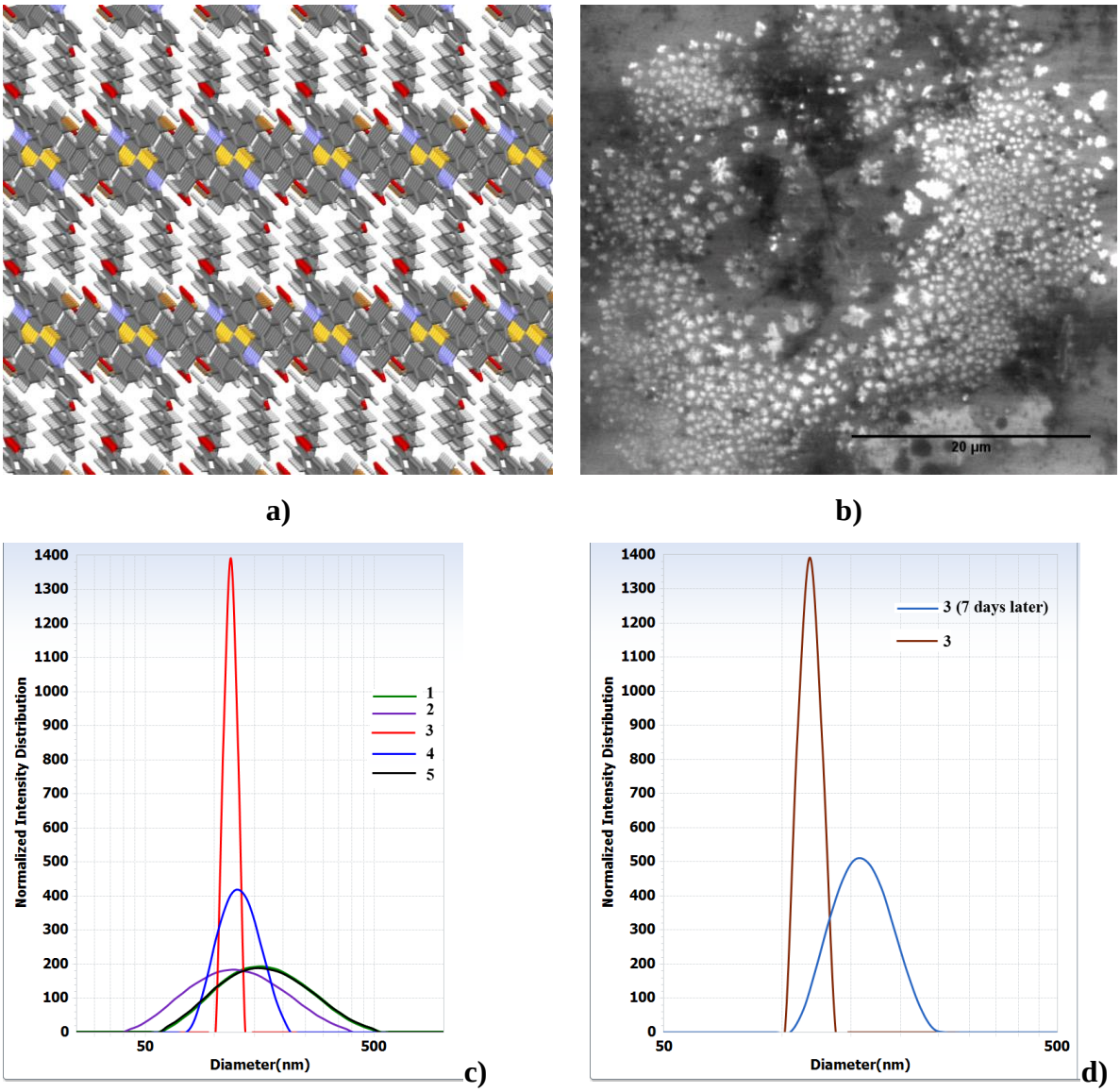

Figure 1. a) X-ray molecular structure of **FhABr**; b) SEM image of the sample **3** casted on glass; c) Distribution of the mean hydrodynamic diameter of the samples **1** – **5**; d) The influence of ageing on the mean hydrodynamic diameter of the sample **3**

The dispersion of the **FhABr** into the **PMMA** and **PF** matrix respectively, led to self-standing films. To investigate the segregation of the **FhABr** in form of nanoparticles into the polymeric matrix, and besides to gain three-dimensional information related to their shape, location, size and distribution, the **1a-6a** and **1b-6b** samples were analysed by scanning electron microscopy (SEM) and atomic force microscopy (AFM).

SEM imaging revealed a smooth surface at micrometric level for all the films. Nanometric round shapes could be distinguished, suggesting that the **FhABr** grew as spherical shapes into the polymeric matrix (Figure 2a,b,c). Compared to the flower-like crystals grown from water (Figure 1b), the spherical shape indicates enough interfacial tension between the

FhABr and the polymeric matrix to force the growing of round nanoparticles. Regarding the variation of the mean diameter of the nanoparticles, in the case of PMMA matrix it was observed a similar trend as for water suspensions; lower diameter values of 160 nm and a standard deviation (SD) of 0.02 were registered for the sample **4a** with a median concentration of **FhABr** (Figure 1s). A less evident correlation has been registered in the case of using PF matrix, when the mean diameter varied from 200 nm up to 350 nm in a random manner, with a lower SD for the samples **1b** and **2b** (Figure 1s). This was attributed to the higher viscosity of the **PF** solution compared to the one of PMMA. In comparison with the nanoparticles formed in water, it could be observed a much narrower polydispersity attributed to the influence of the viscous polymer solution which hinders the mobility of the nanocrystals and thus their aggregation. Related to the dimension of the nanoparticles measured by SEM, it should be considered that the **FhABr** nanocrystals were covered by a polymer shell, and their real dimension were lower [30]. To have an insight at nanometric level, the films surface has been scanned by AFM, topographic and phase contrast methods. The surface of the PMMA based films was very smooth, with roughness between 2.6 and 48 nm, while those based on PF were rougher, with roughness between 29 and 129 nm (Table 2s). On the surface, well defined spherical shapes were monitored, with similar diameters as measured by SEM. The AFM phase contrast images confirmed the lower real dimension of the nanoparticles, with diameter values less than 105 nm (Table 3s).

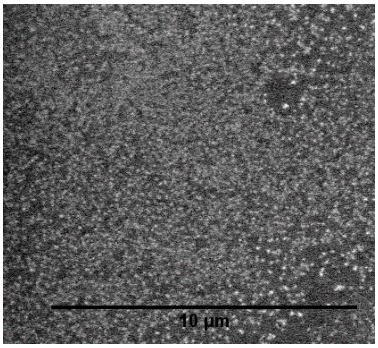

a) **2a**

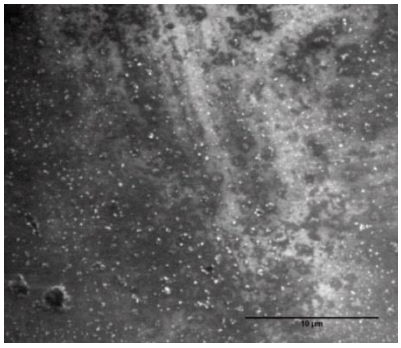

b) **4a**

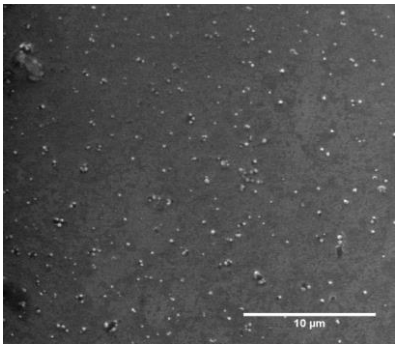

c) **1b**

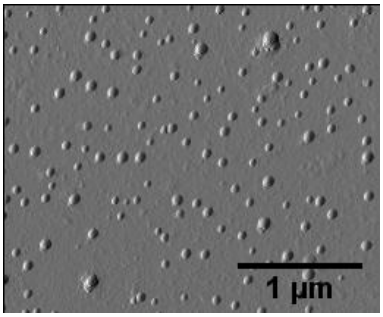

d) **2a**

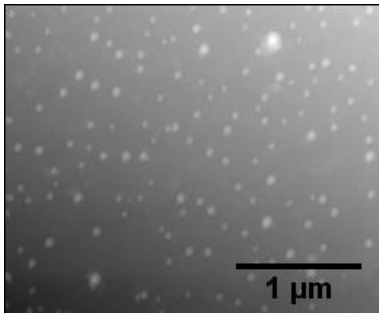

e) **2a,** phase contrast

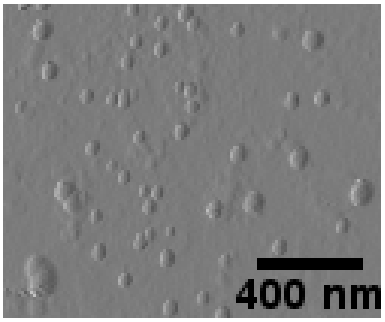

f) **2a**

Figure 2. Representative images of the film samples, acquired by SEM (a,b,c) and AFM (d,e,f)

To confirm the supramolecular ordering of the nanoparticles, the samples were visualized by polarized light microscopy. The crystalline **FhABr**, as recrystallized from solution, showed under polarized light sharp wedge geometrical shapes with strong birefringence (Figure 3a) [11]. When dispersed as nanoparticles into the polymer matrix, it appeared as birefringent round droplets with different coloured concentric rings (Figure 3b), a texture usually developed by the layered supramolecualar arrangement of a smectic A mesophase in bulk or when dispersed into a polymer matrix [35-37]. Its occurring is in agreement with the tendency of layered self-organization of the **FhABr** molecules, driven by the rigid-flexible segregation (Figure 1a). The birefringent droplets could be seen in both polymer matrices, more difficult to be distinguished into PF because of its own birefringence (Figure 3b-d) [38]. The birefringent droplets confirmed the crystalline structure of the **FhABr** nanoparticles as indicated by SEM and AFM microscopy. Moreover, a closer view of the droplets reveals an extension of the birefringent concentric rings into the polymeric matrix surrounding the **FhABr** nanocrystals, signature of a coupling of the ordering at interface [36, 39]. Thus, it is expected that the **FhABr** nanocrystals to be strongly anchored into the PMMA and PF polymeric matrix by the interfacial forces.

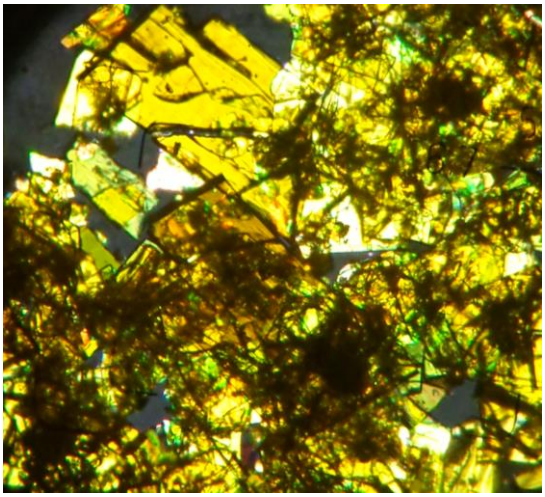

a) FhABr, (200x)

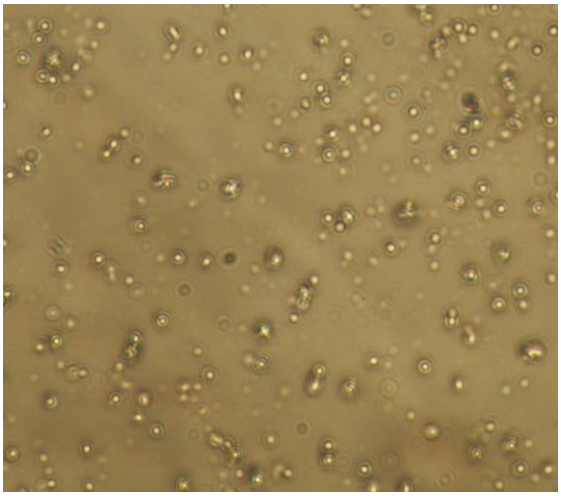

b) 3a, (200x)

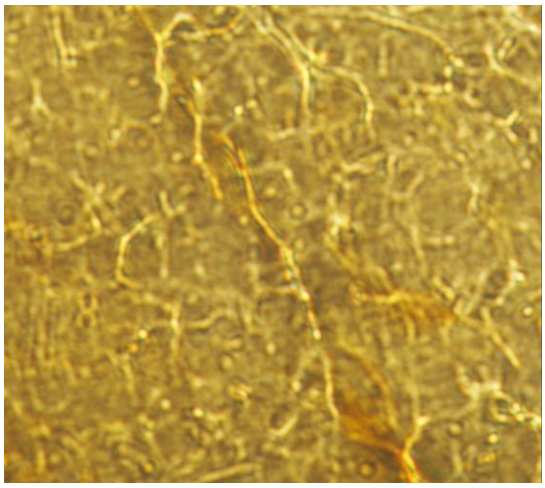

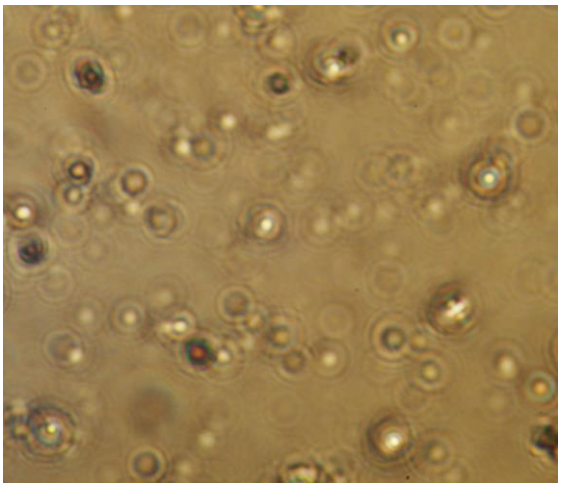

c) 3b, (200x) **d) 2a,** (400x)

Figure 3. Polarized light microscopy of a) the **FhABr** single crystals and b-d) **FhABr** dispersed in PMMA and PF matrix (the magnification is given in brackets)

Photophysical behavior

1. The UV-vis spectrum of the **FhABr** solution in THF ($1.33x10^{-5}$M) exhibited four absorption maxima. The two maxima at lower wavelength, at 273 and 293 nm, were attributed to the spin allowed π-π* benzenoid transitions of the local aromatic units. The two maxima at higher wavelength, at 342 and 395 nm, were attributed to the localized conjugated system between the phenothiazine donor (D) and the formyl acceptor (A), and to the D-A intramolecular charge transfer complex (ICT) respectively (Figure 4a) [40]. By comparison, the absorption spectra of the **FhABr** nanocrystals in water revealed a bathochromic shift of the absorption maxima (to 277, 299, 348 and 404 nm), suggesting electronic transitions to lower state, characteristic to a head-to-tail arrangement of a J-type coupling into nanocrystals (Figure 4b, Figure 2s) [40]. The absorption intensity characteristic to the π-π* benzenoid transitions slightly decreased, while the absorption intensity characteristic to the conjugated system and to the intramolecular charge transfer (ICT) slightly increased. This is in agreement with the restriction of the intramolecular rotations in solid state which favoured the better conjugation and ICT from phenothiazine donor to formyl acceptor [41]. The absorption maxima followed a progressive bathochromic shifting as the suspensions aged and further for the crystalline films (Figure 4b), in agreement with the enhanced intermolecular forces as the crystal size increased [41, 42].

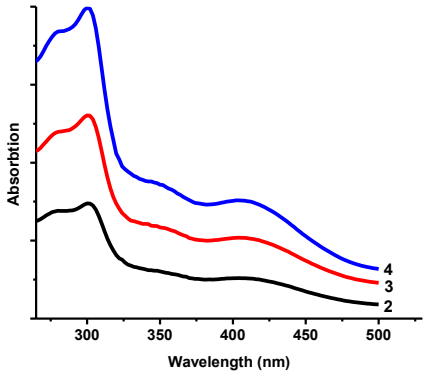

2.

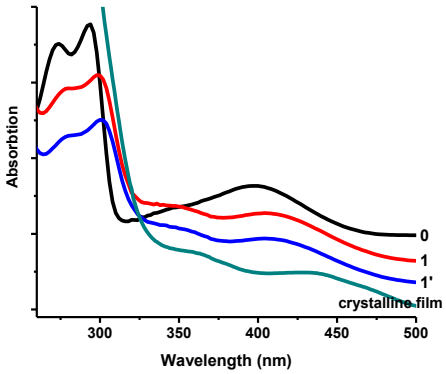

4.

3. a)

5. b)

6. **Figure 4**. a) Absorption spectra of the nanocrystals samples in water (**2**, **3**, **4)** and b) Comparative absorption spectra of the **FhABBr** in different states: solution in THF (**0**), nanocrystals in water (**1**), nanocrystals in water aged for one week (**1'**) and crystalline film

To establish the influence of the nanocrystallization on the luminescence properties, the emission spectra of the **FhABBr** nanocrystals dispersed in water, and PMMA and PF polymer matrix were recorded, by exciting with the absorption maxima of 348 and 404 nm. The spectra of the **FhABBr** solution, and pristine PMMA and PF films were recorded also as reference. At first, no influence of the excitation wavelength on the emission profile was noted (Figure 5, Figure 3s). The emission spectrum of the **FhABBr** nanocrystals in water and PMMA had a similar shape to that of the **FhABBr** solution, with the main difference of a blue shifting of 10 nm and 35 nm respectively, from 535 nm to 525 and 500 nm (Figure 5). This blue shifting of the emission was attributed to the interfacial phenomena, which affected the **FhABBr** ordering into the crystalline state [23, 24, 29, 30, 43], and also to the different size of the nanocrystals [44, 45]. A similar behaviour was observed in the case of the hydrogels obtained by the formation of phenothiazine ordered clusters into the aqueous matrix [46]. On the contrary, the emission of the **FhABBr** bulk crystals was red shifted (545 nm) compared to that of the **FhABBr** solution, clearly indicating the influence of the surrounding medium on the supramolecular ordering (Figure 5). This influence was more evident for the **FhABBr** nanocrystals in PF, which showed an emission spectrum similar to that of the pristine PF matrix, with three emission maxima (466, 493, 538 nm) slightly red shifted around 7 nm.

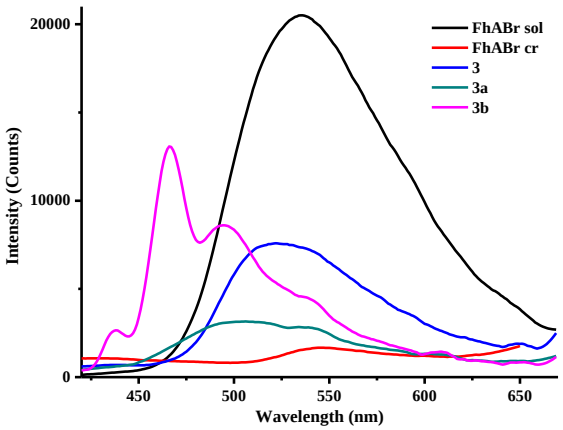

Figure 5. Comparative emission spectra of **FhABr** solution and **FhABr** nanocrystals in water (**3**), PMMA (**3a**) and PF (**3b**), excited at 348 nm

The intensity of the emission was drastically affected by the nature of the supramolecular ordering of the **FhABr**: it was the highest in the case of the isolated molecules in solution, the lowest for the bulk crystalline state and medium for the nanocrystals, both in water or polymer matrix. The variation of the concentration of the **FhABr** into the water suspensions and polymer films didn't significantly affect the emission profile (Figure 6a, b, c), but significantly influenced the emission intensity. Interesting enough, the emission intensity was correlated with the size of the nanocrystals and not with the content of the chromophore; the highest emission intensity has been recorded for the nanocrystals with the lowest size.

While no significant influence of the excitation wavelength was observed on the emission profile, its drastic influence has been registered on the emission intensity, quantified by measuring of the quantum yield (Table 3, Table 4). The **FhABr** nanocrystals showed, in a similar manner with the THF solution and bulk crystalline state, that the excitation with the absorption maximum of the intramolecular charge-transfer (ICT) band resulted in a more effective fluorescence than the excitation with the absorption maximum of the conjugated system. It is expected that the interaction of the **FhABr** chromophore with the polar environment (THF, PMMA) to stabilize its planar intramolecular charge transfer state by diminishing the torsion motions around the single bonds [47, 48]. Considering the larger intermolecular distances between the phenothiazine cores, the improvement of the quantum yield when excited with the lower ICT energy should be attributed to the weakening of the non-radiative de-excitation channels. This should be favoured by the diminishing of the excimer formation by π-π stacking and of the energy dissipation to the surrounding environment.

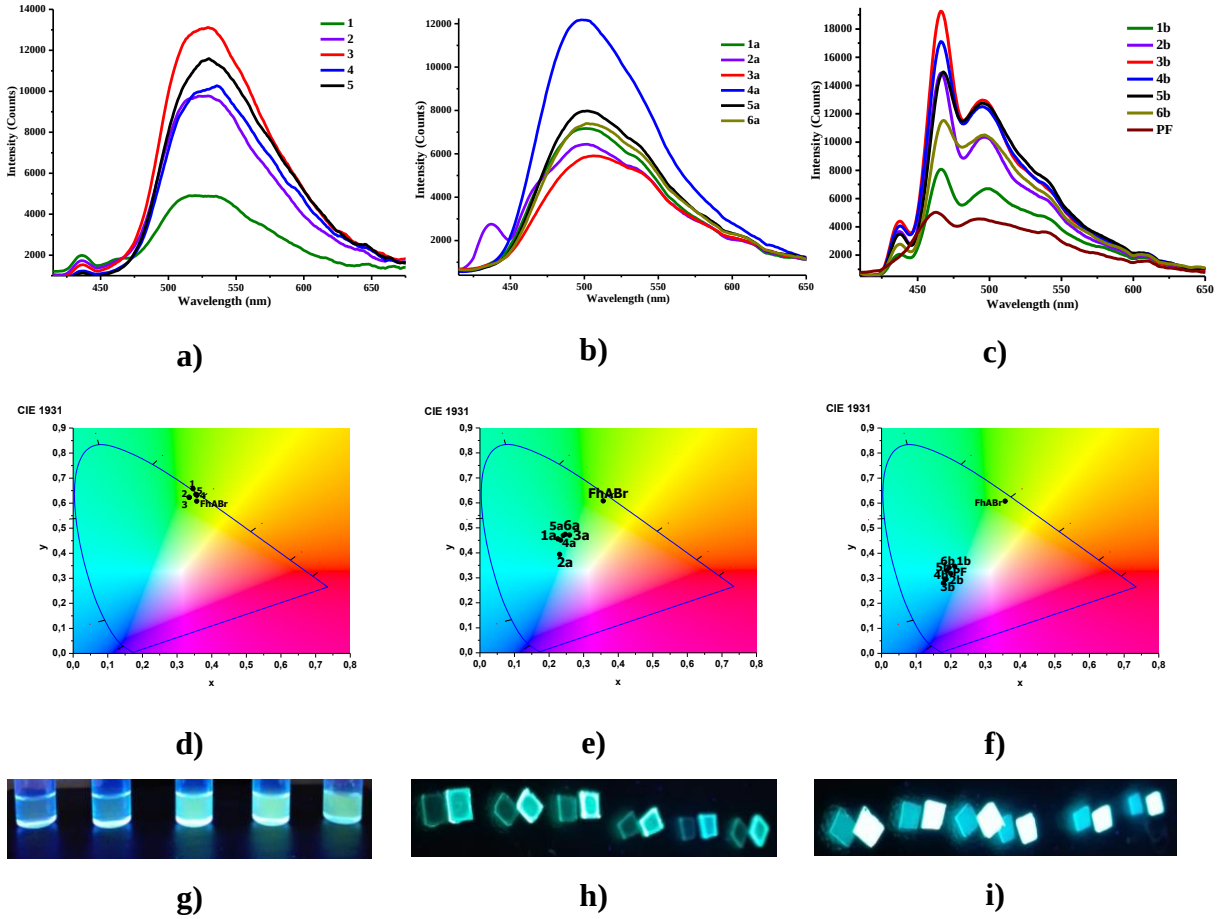

Figure 6. Emission spectra, chromaticity diagram and images of the samples illuminated with an UV lamp of the nanocrystals in a), d), g) water, b), e), h) PMMA and c), f), i) PF, when excited at 395 nm

Comparing the emission of the **FhABr** nanocrystals in water to that of the **FhABr** bulk crystal, it could be observed an amazing increase of the luminescence efficiency attributed to the nano-size, which increased the surface-to-volume ratio [2]. Among the **1-5** samples, it was observed a variation of the luminescence intensity inversely proportional with the variation of the nanocrystals size and their polydispersity; better quantum yield was registered for smaller nanoparticles with narrower polydispersity (Figure 7). A similar trend was also reported for nanocrystals of polyfluorene, and was attributed to the increase of the surface-to-volume ratio, to the better quality of the small crystals, and their ability to accelerate the emission [2].

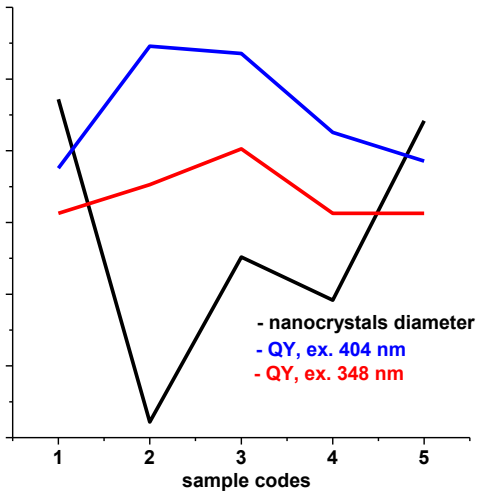

Figure 7. Graphical representation of the variation of the size of the nanocrystals in water (black) *versus* their quantum yield when excited with 348 (red) and 404 nm (blue)

Table 3. Quantum yield (**QY**) of the **FhABr** in solution, nanocrystals in water and bulk crystal

Code	mol/L	**QY** (λ_{ex} = 348 nm)	**QY** (λ_{ex} = 404 nm)
0	$1.33 * 10^{-5}$	24.8	54.6
1	$0.66*10^{-5}$	11.3	18.7
2	10^{-5}	15.4	35.4
3	$1.33 * 10^{-5}$	20.06	34.7
4	$2 *10^{-5}$	11.64	23.51
5	$2.66 * 10^{-5}$	11.73	19.43
FhABr	bulk crystal	2.12	4.2

A similar behaviour was observed for the film samples of the **FhABr** nanoparticles dispersed into the polymeric matrix of PMMA and PF. The quantum yield provided lower values when excited with the wavelength of the absorption maximum of the conjugated system, and higher values when excited with the wavelength corresponding to the intramolecular charge transfer (Table 4). A maximum value of the quantum yield of 45% was reached for the films in PMMA matrix and one of 39% for the films in polyfluorene. The values significantly surpass those of the pure components, **FhABr** and polymer matrix, when excited with light of similar wavelength.

7. When excited with light of wavelength corresponding to the conjugated system, the nanoparticles dispersed in PMMA presented lower values of the quantum yield compared to those in water. This was attributed to the luminescence quenching because of the transfer of the excited electrons of **FhABr** to the ester groups of PMMA, which play the role of acceptor sites [49]. The intermolecular charge transfer seems to be avoided when the **1a-6a** samples were excited with the energy corresponding to the intramolecular charge transfer of **FhABr**, when

the quantum yield has higher values in PMMA films compared to those of the nanocrystals in water. The explanation can be given by the disagreement between the HOMO/LUMO orbitals of the **FhABr** and PMMA [49].

8.

Table 4. Quantum yield of the **FhABr** nanocrystals in PMMA (**1a-6a**) and PF (**1b-6b**)

Code	QY (λ_{ex} = 348 nm)	QY (λ_{ex} = 404 nm)
PMMA/PF	0 / 7.01	0 / 19.07
1a/1b	8.17 / 9.37	35.98 / 26.93
2a/2b	7.2 / 13.29	31.4 / 32.44
3a/3b	7.12 / 18.06	27.55 / 39.04
4a/4b	11.21 / 17.25	45.38 / 37.28
5a/5b	9.41 / 16.72	33.14 / 38.68
6a/6b	9.44 / 14.64	31.44 / 36.25
FhABr bulk crystal	2.12	4.2

As can be seen in figure 6, all the samples emitted light in the gamut of human vision. The blue shifting of the emission was reflected in the shifting of the colour of the emitted light: from green-yellowish (**FhABr** solution) to green (**FhABr** nanocrystals in water), green-bluish (**FhABr** nanocrystals in PMMA) and blue (**FhABr** nanocrystals in PF).

Conclusions

Nanocrystals based on a phenothiazine chromophore were successfully prepared, in both water and a polymeric matrix, namely polymethylmethacrylate and polyfluorene. Nanocrystals with diameter around 113 nm were obtained by reprecipitation in water, and around 105 nm by solvent induced phase separation in PMMA and PF matrix. They presented high efficient luminescence when excited with visible light, reaching an absolute quantum yield of 35 % in water, 45 % in PMMA, and 39 % in polyfluorene.

The high luminescence efficiency of the nanoparticles in the water biodispersant, when excited with light of low energy makes them attractive for bio-applications, while the high efficiency of the nanoparticles in solid films recommends them as reliable candidates for optoelectronics.

Acknowledgements

The paper is part of a project financed through a Romanian National Authority for Scientific Research MEN – UEFISCDI grant, project number PN-III-P1-1.2-PCCDI2017-0917.

References

1. A. M. Smith, S. Nie, **S**emiconductor nanocrystals: structure, properties, and band gap engineering, *Acc. Chem. Res*. **2010**, 43, 190-200.
2. D. Tuncel, H. V. Demir, Conjugated polymer nanoparticles, *Nanoscale*. **2010**, 2, 484-494.
3. D. Li, W. Qin, B. Xu, J. Qian, B. Z. Tang, AIE nanoparticles with high stimulated emission depletion efficiency and photobleaching resistance for long-term super-resolution, *Adv. Mater*. **2017**, 29, Article Number: 1703643.
4. J-U. A. H. Junghanns, R. H. Müller, Nanocrystal technology, drug delivery and clinical applications, *Int. J. Nanomedicine*. **2008**, 3, 295-310.
5. C. Shahar, J. Baram, Y. Tidhar, H. Weissman, S. R. Cohen, I. Pinkas, B. Rybtchinski, Self-assembly of light-harvesting crystalline nanosheets in aqueous media, *ACS Nano* **2013**, 7, 3547-3556.
6. S. Rosenne, E. Grinvald, E. Shirman, L. Neeman, S. Dutta, O. Bar-Elli, R. Ben-Elli, R. Zvi, E. Oksenberg, P. Milko, V. Kalchenko, H. Weissman, B. Rybtchinski, Self-assembled organic nanocrystals with strong nonlinear optical response, *Nano Lett*. **2015**, 15, 7232-7237.
7. S.M.A. Fateminia, Z. Wang, C.C. Goh, P.N. Manghnani, W. Wu, D. Mao, L. G. Ng, Z. Zhao, B.Z. Tang, B. Liu, Nanocrystallization: a unique approach to yield bright organic nanocrystals for biological applications, *Adv. Mater*. **2016**, 29, 1604100.
8. S.M.A. Fateminia, Z. Mao, S. Xu, Z. Yang, Z. Chi, B. Liu, Organic nanocrystals with bright red persistent room-temperature phosphorescence for biological applications, *Angew. Chem. Comm*. **2017**, 129, 12328-12332.
9. P-Z. Chen, Y-X. Weng, L-Y. Niu, Y-Z. Chen, L-Z. Wu, C.-H. Tung, Q-Z. Yang, Light-harvesting systems based on organic nanocrystals to mimic chlorosomes, *Angew. Chem. Int. Ed*. **2016**, 55, 275-2763.
10. Y. Zhan, Y. Xu, Z. Jin, W. Ye, P. Yang, Phenothiazine substituted phenanthroimidazole derivatives: Synthesis, photophysical properties and efficient piezochromic luminescence, *Dyes Pigm.* **2017**, 140, 452-459.
11. A. Bejan, S. Shova, M. D. Damaceanu, B. C. Simionescu, L. Marin, Structure-directed functional properties of phenothiazine brominated dyes: morphology and photophysical and electrochemical properties, *Cryst. Growth Des.* **2016**, *16*, 3716-3730.
12. A. Zabulica, M. Balan, S. Belei, M. Sava, B. C. Simionescu, L. Marin, Novel luminescent phenothiazine-based Schiff bases with tuned morphology. Synthesis, structure, photophysical and thermotropic characterization, *Dyes Pigm.* **2013**, 96, 686-692.

13. F. Xu, C. Wang, L. Yang, S. Yin, A. Wedel, S. Janietz, H. Krueger, Y. Hua, PPV-derivatives containing phenothiazine and alkyloxy-substituted oxadiazole/Phenyl units for OLED, *Synthetic Met*. **2005**, 152, 221-224.
14. H. Cao, Z. Chen, Y. Liu, B. Qu, S. Xu, S. Cao, Z. Lan, Z. Wang, Q. Gong, Undoped yellow-emitting organic light-emitting diodes from a phenothiazine-based derivative, *Synthetic Met*. **2007**, 157, 427-431.
15. L. Marin, A. Bejan, D. Ailincai, D. Belei, Poly(azomethine-phenothiazine)s with efficient emission in solid state, *Eur. Polym. J.* **2017**, 95, 127-137.
16. S.J. Ananthakrishnan, E. Varathan, V. Subramanian, N. Somanathan, A.B. Mandal, White light emitting polymers from a luminogen with local polarity induced enhanced emission, *J. Phys. Chem. C* **2014**, 118, 28084-28094.
17. X. H. Zhang, S. H. Choi, D. H. Choi, K. H. Ahn, Synthesis and photophysical properties of phenothiazine-labeled conjugated dendrimers, *Tetrahedron Lett*. **2005**, 46, 5273-5276.
18. C. Arivazhagan, A. Maity, K. Bakthavachalam, A. Jana, A. Chowdhury, S. K. Panigrahi, E. Suresh, P.S. Mukherjee, A. Das, S. Ghosh, Phenothiazinyl boranes: a new class of AIE luminogens with mega Stokes shift, mechanochromism and mechanoluminescence, *Chem. Eur. J.* **2017**, 23, 7046-7051.
19. D. Belei, C. Dumea, E. Bicu, L. Marin, Phenothiazine and pyridine-N-oxide-based AIE-active triazoles: synthesis, morphology and photophysical properties, *RSC Adv.* **2015**, 5, 8849-8858.
20. S. Brovelli, W.K. Bae, C. Galland, U. Giovanella, F. Meinardi, V.I. Klimov, Dual-color electroluminescence from dot-in-bulk nanocrystals, *Nano Lett.* **2014**, 14, 486-494.
21. G. Leone, G. Ricci, T. Virgili, I.S. Lopez, S.K. Rajendranb, C. Botta, U. Giovanella, Oxazine- J-aggregates in polymer nanohybrids, *Phys. Chem. Chem. Phys*. **2012**, 14, 13646-13650.
22. J. Moreau, U. Giovanella, J.P. Bombenger, W. Porzio, V. Vohra, L. Spadacini, G. Di Silvestro, L. Barba, G. Arrighetti, S. Destri, M. Pasini, M. Saba, F. Quochi, A. Mura, G. Bongiovanni, M. Fiorini, M. Uslenghi, C. Botta, Highly emissive nanostructured thin films of organic host-guests for energy conversion. *Chemphyschem*. **2009**, 10, 647-53.
23. R. Liu, H. Wang, W. J. Jin, Soft-cavity-type host-guest structure of cocrystals with good luminescence behavior assembled by halogen bond and other weak interactions, *Cryst. Growth Des.* **2017**, 17, 3331-3337.

24. D.B. Tada, L.M. Rossi, C.A.P. Leite, R. Itri, M.S. Baptista, Nanoparticle platform to modulate reaction mechanism of phenothiazine photosensitizers, *J. Nanosci. Nanotechno*. **2010**, 10, 3100-3108.
25. L.S. Chougala, J.S. Kadadevarmath, A.A. Kamble, P.K. Bayannavar, M.S. Yatnatti, R.K. Linganagoudar, J.M. Nirupama, R.R. Kamble, Q. Qiao, Effect of TiO2 nanoparticles on newly synthesized phenothiazine derivative-CPTA dye and its applications as dye sensitized solar cell, *J. Mol. Liq*. **2017**, 244, 97-102.
26. J. Kong, J. Yang, Z. Xue, H. Zhou, L. Cheng, Q. Zhang, J. Wu, B. Jin, S. Zhang, Y. Tian, Regulation of luminescence band and exploration of antibacterial activity of a nanohybrid composed of fluorophore-phenothiazine nanoribbons dispersed with Ag nanoparticles, *J. Mat. Chem. C* **2013**, 1, 5047-5057.
27. L.R.S. Barbosa, R. Itri, W. Caetano, Self-assembling of phenothiazine compounds investigated by small-angle X-ray scattering and electron paramagnetic resonance spectroscopy, *J. Phys. Chem. B* **2008**, 112, 4261-4269.
28. E. Perju, L. Marin, V.C. Grigoras, M. Bruma, Thermotropic and optical behaviour of new PDLC systems based on a polysulfone matrix and a cyanoazomethine liquid crystal, *Liq. Cryst*. **2011**, 7, 893-905.
29. L. Marin, A. Zabulica, I.A. Moleavin, Luminescent guest-host composite films based on an azomethine dye in different matrix polymers, *Opt. Mat*. **2014**, 38, 290-296.
30. K.P. Morak-Mlodawska, M. Jeleń, Recent progress in biological activities of synthesized phenothiazines, *Eur. J. Med. Chem*. **2011**, 46, 3179-3189.
31. F. Khan, D. Kumar, N. Azum, M. A. Rub, A.M. Asiri, Effect of salt and urea on complexation behavior of pharmaceutical excipient gelatin with phenothiazine drug promazine hydrochloride, *J. Mol. Liq*. **2015**, 208, 84-91.
32. C. Chang, C.K. Chou, I.J. Chang, Y.P. Lee, E. W.G. Diau, Relaxation Dynamics of Ruthenium Complexes in Solution, PMMA and TiO2 Films: The Roles of Self-Quenching and Interfacial Electron Transfer, *J. Phys. Chem. C* **2007**, 111, 13288-13296.
33. Z. Ma, P. Sonar, Z.K. Chen, Recent progress in fluorescent blue light-emitting materials, *Curr. Org. Chem*. **2010**, 14, 2034-2069.
34. C. Wu, Y. Zheng, C. Szymanski, J. McNeill, Energy transfer in a nanoscale multichromophoric system: fluorescent dye-doped conjugated polymer nanoparticles, *J. Phys. Chem. C* **2008**, 112, 1772-1781.
35. M. Baron, Definitions of basic terms relating to low-molar-mass and polymer liquid crystals, *Pure Appl. Chem*. **2001**, 73, 845-895.

36. D. Ailincai, C. Farcau, E. Paslaru, L. Marin, PDLC composites based on polyvinyl boric acid matrix - a promising pathway towards biomedical engineering, *Liq. Cryst*. **2016**, 43, 1973-1985.
37. N. Pongali Sathya Prabu, M.L.N. Madhu Mohan, Characterization of a new smectic ordering in supramolecular hydrogen bonded liquid crystals by X-ray, optical and dielectric studies, *J. Mol. Liq*. **2013**, 182, 79-90.
38. S.H. Yang, C.S. Hsu, Liquid crystalline conjugated polymers and their applications in organic electronics, *J. Polym. Sci. A.* **2009**, 47, 2713-2733.
39. J.M. Brake, N.L. Abbott, Coupling of the orientations of thermotropic liquid crystals to protein binding events at lipid-decorated interfaces, *Langmuir* **2007**, 23, 8497-8507.
40. A. Liess, A. Lv, A. Arjona-Esteban, D. Bialas, A.M. Krause, V. Stepanenko, M. Stolte, F. Würthner, Exciton coupling of merocyanine dyes from H- to J-type in the solid state by crystal engineering, *Nano Lett.* **2017**, 17, 1719-1726.
41. Y. Hong, J. W. Y. Lama, B. Z. Tang, Aggregation-induced emission: phenomenon, mechanism and applications, *Chem. Commun.* **2009**, 0, 4332-4353.
42. R. Yoshii, A. Hirose, K. Tanaka, Y. Chujo, Boron Diiminate with Aggregation-Induced Emission and Crystallization-Induced Emission-Enhancement Characteristics, *Chem. - Eur. J.* **2014**, 20, 8320-8324.
43. M.S. Ali, H.A. Al-Lohedan, Interaction of biocompatible polymers with amphiphilic phenothiazine drug chlorpromazine hydrochloride, *J. Mol. Liq*. **2013**, 177, 283-287.
44. H. Tanaka, K. Shizu, H. Nakanotani, C. Adachi, Dual intramolecular charge-transfer fluorescence derived from a phenothiazine-triphenyltriazine derivative, *J. Phys. Chem. C* **2014**, 118, 15985-15994.
45. M.L. Mastronardi, F. Maier-Flaig, D. Faulkner, E.J. Henderson, C. Kübel, U. Lemmer, G.A. Ozin, Size-Dependent Absolute Quantum Yields for Size-Separated Colloidally-Stable Silicon Nanocrystals, *Nano Lett.* **2012**, 12, 337-342.
46. A. Bejan, D. Ailincai, B.C. Simionescu, L. Marin, Chitosan hydrogelation with a phenothiazine based aldehyde – toward highly luminescent biomaterials, *Polym. Chem*. **2018**, 9, 2359-2369.
47. H. Zhu, M. Li, J. Hu, X. Wang, J. Jie, Q. Guo, C. Chen, A. Xia, Ultrafast investigation of intramolecular charge transfer and solvation dynamics of tetrahydro[5]-helicene-based imide derivatives, *Sci. Rep. UK* **2016**, 6, 24313

48. R. Chen, Y. Gao, G. Zhang, R. Wu, L. Xiao, S. Jia, Electric field induced fluorescence modulation of single molecules in pmma based on electron transfer, *Int. J. Mol. Sci.* **2012**, 13, 11130-11140.
49. S. H. Ko, C. H. Yoo, T. W. Kim, Electrical bistabilities and memory stabilities of organic bistable devices utilizing C60 molecules embedded in a polymethyl methacylate matrix with an Al2O3 blocking layer, *J. Electrochem. Soc*. **2012**, 159, G93-G96.

Supplementary Information

Phenothiazine based nanocrystals with enhanced solid state emission

Andrei Bejan, Luminita Marin*

"Petru Poni" Institute of Macromolecular Chemistry of Romanian Academy, Iasi, Romania
*lmarin@icmpp.ro

Table 1s. Mean diameter and polydispersity index of the samples **0** – **5**

Code	Mean Diameter*	Polydispersity index*	Mean Diameter**	Polydispersity index**
0	-	-	-	-
1	158	0.2	985	0.4
2	113	0.15	192	0.09
3	136	0.09	192	0.11
4	130	0.145	211	0.14
5	155	0.207	220	0.15

* measured on fresh suspensions; **measured on suspensions kept 1 week

Table 2s. Average roughness of the **1a-6a** and **1b-6b** samples, measured by AFM*

Matrix	Cod	Ra	Matrix	Cod	Ra
PMMA	**1a**	9.8 nm	***PFL***	**1b**	129.6 nm
	2a	2.6 nm		**2b**	29.9 nm
	3a	48.6 nm		**3b**	60.1 nm
	4a	48.8 nm		**4b**	-**
	4a	45nm		**5b**	-**
	6a	17.7 nm		**6b**	-**

*Read on 30x30 μm^2; **couldn't be measured

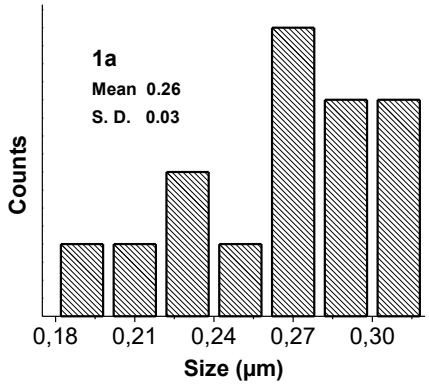
1a
Mean 0.26
S. D. 0.03
Counts
0,18 0,21 0,24 0,27 0,30
Size (µm)

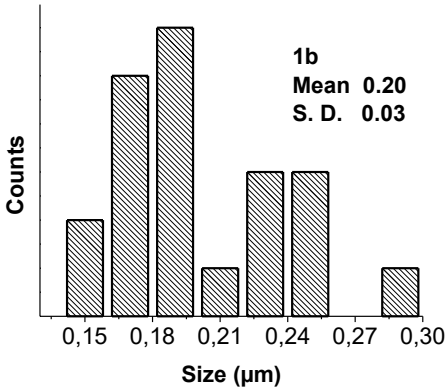
1b
Mean 0.20
S. D. 0.03
Counts
0,15 0,18 0,21 0,24 0,27 0,30
Size (µm)

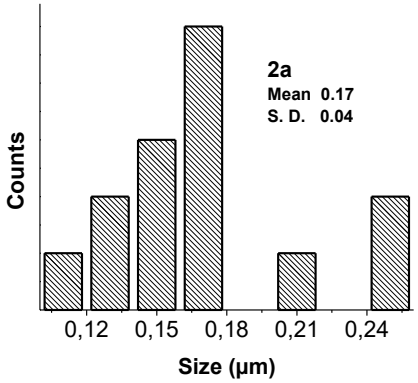
2a
Mean 0.17
S. D. 0.04
Counts
0,12 0,15 0,18 0,21 0,24
Size (µm)

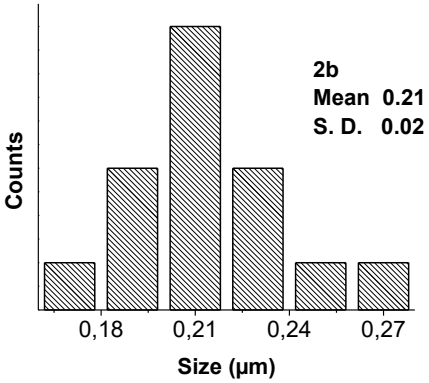
2b
Mean 0.21
S. D. 0.02
Counts
0,18 0,21 0,24 0,27
Size (µm)

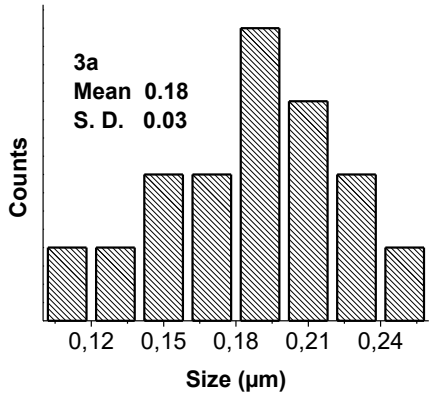
3a
Mean 0.18
S. D. 0.03
Counts
0,12 0,15 0,18 0,21 0,24
Size (µm)

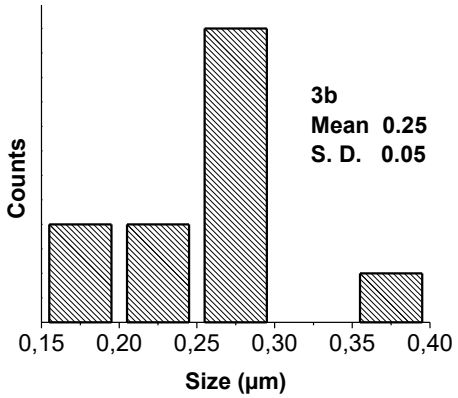
3b
Mean 0.25
S. D. 0.05
Counts
0,15 0,20 0,25 0,30 0,35 0,40
Size (µm)

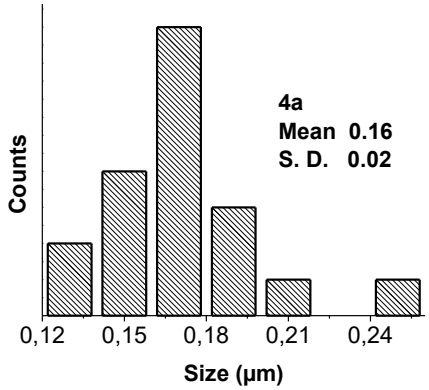
4a
Mean 0.16
S. D. 0.02
Counts
0,12 0,15 0,18 0,21 0,24
Size (µm)

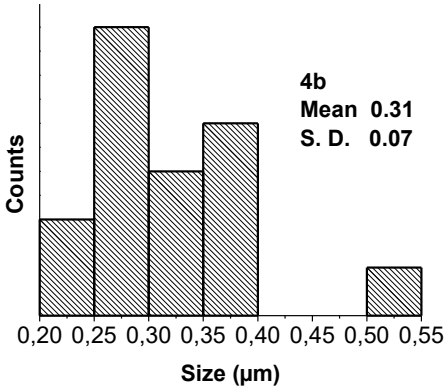
4b
Mean 0.31
S. D. 0.07
Counts
0,20 0,25 0,30 0,35 0,40 0,45 0,50 0,55
Size (µm)

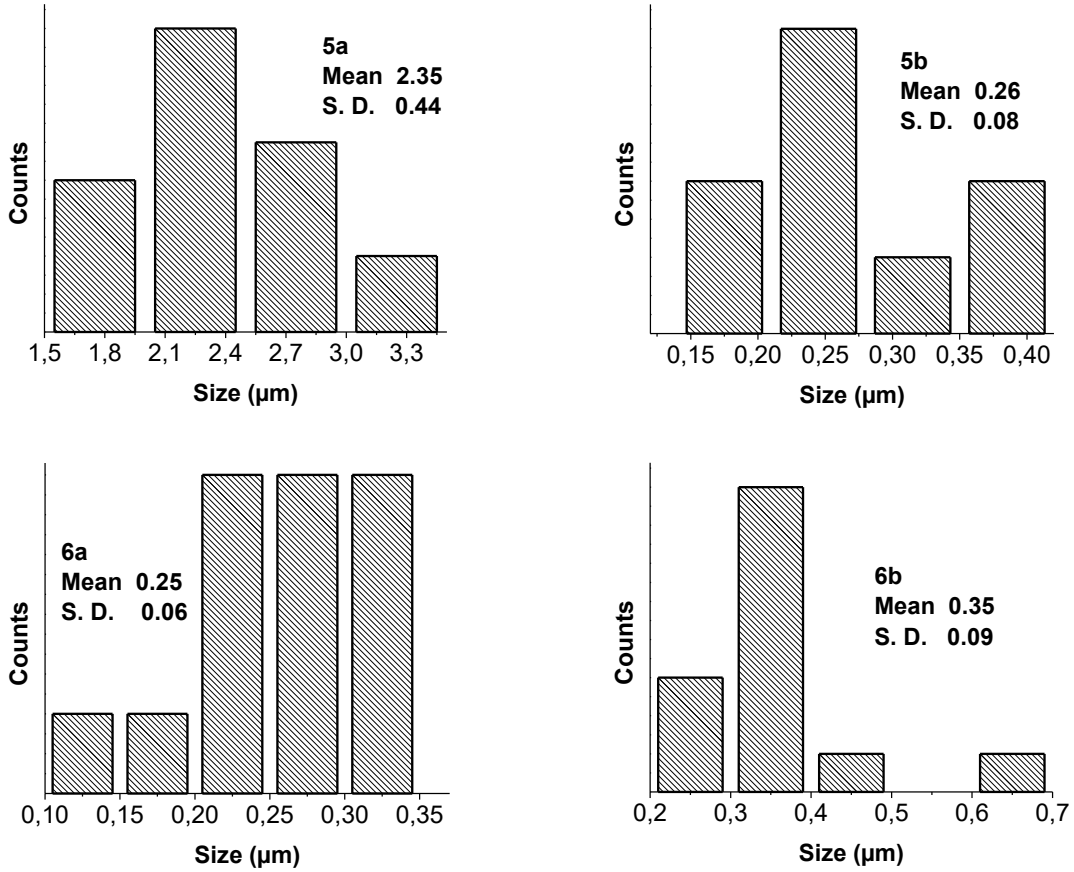

Figure 1s. Diameter size distribution and standard deviation (S.D.) of the samples **1a**-**6a** si **1b**-**6b**

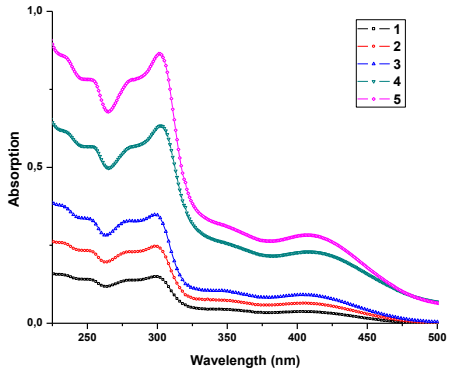

Figure 2s. Absorption spectra of the nanocrystals in water

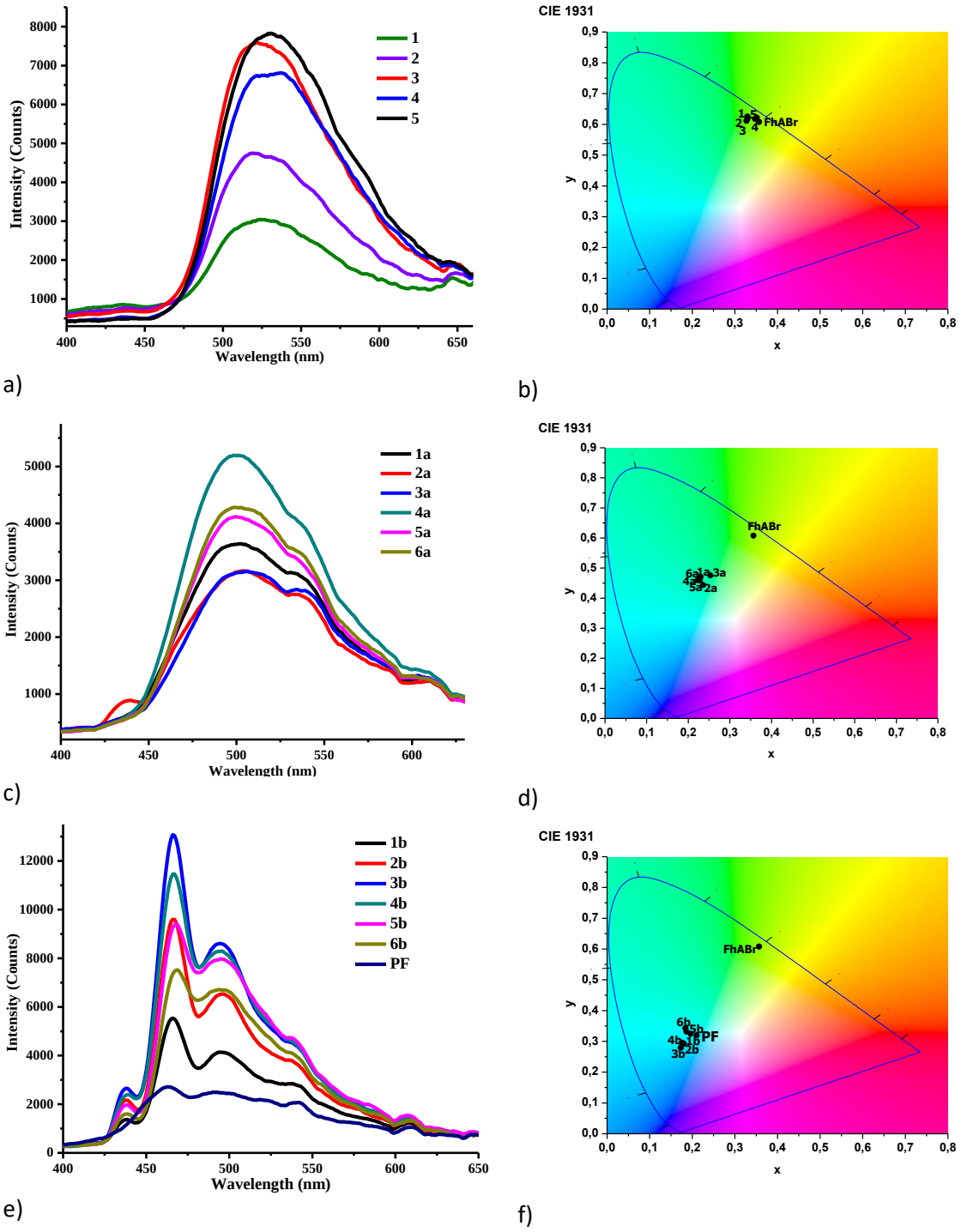

Figure 2s. Emission spectra and chromaticity diagrams of the nanocrystals in a),b) water; c),d) PMMA and e), f) PF, when excited with 348 nm